© 2014. Published by The Company of Biologists Ltd | Development (2014) 141, 3177-3187 doi:10.1242/dev.107433

RESEARCH ARTICLE

p120-catenin-dependent junctional recruitment of Shroom3 is required for apical constriction during lens pit morphogenesis

Richard A. Lang[1], Ken Herman[2], Albert B. Reynolds[3], Jeffrey D. Hildebrand[4] and Timothy F. Plageman, Jr[2,*]

ABSTRACT

Apical constriction (AC) is a widely utilized mechanism of cell shape change whereby epithelial cells transform from a cylindrical to conical shape, which can facilitate morphogenetic movements during embryonic development. Invertebrate epithelial cells undergoing AC depend on the contraction of apical cortex-spanning actomyosin filaments that generate force on the apical junctions and pull them toward the middle of the cell, effectively reducing the apical circumference. A current challenge is to determine whether these mechanisms are conserved in vertebrates and to identify the molecules responsible for linking apical junctions with the AC machinery. Utilizing the developing mouse eye as a model, we have uncovered evidence that lens placode AC may be partially dependent on apically positioned myosin-containing filaments associated with the zonula adherens. In addition we found that, among several junctional components, p120-catenin genetically interacts with Shroom3, a protein required for AC during embryonic morphogenesis. Further analysis revealed that, similar to Shroom3, p120-catenin is required for AC of lens cells. Finally, we determined that p120-catenin functions by recruiting Shroom3 to adherens junctions. Together, these data identify a novel role for p120-catenin during AC and further define the mechanisms required for vertebrate AC.

KEY WORDS: Shroom3, Apical constriction, Invagination, Lens pit morphogenesis, p120-catenin, delta1 catenin (Ctnnd1)

INTRODUCTION

To generate the three-dimensional shape of an embryo requires epithelial cell sheets to bend and fold in precise and coordinated movements. Epithelial folding events can be facilitated by the direct modification of individual cell geometry, which utilizes forces generated by the cytoskeleton. One such transformative change is apical constriction (AC), a process whereby epithelial cells shorten their apical borders with neighboring cells through the contraction of actomyosin filaments, converting a cell from a cylindrical to a conical shape (Sawyer et al., 2010). Because numerous morphogenetic processes, such as neural tube closure, gastrulation, branching, gut looping and lens pit invagination, are all associated with AC (Lee et al., 2007; Plageman et al., 2010, 2011a; Suzuki et al., 2012; Kim et al., 2013), it is important to elucidate the mechanisms driving this process.

[1]The Visual System Group, Division of Pediatric Ophthalmology and Developmental Biology, Children's Hospital Research Foundation, University of Cincinnati, Cincinnati, OH 45229, USA. [2]College of Optometry, The Ohio State University, Columbus, OH 43210, USA. [3]Department of Cancer Biology, Vanderbilt University, Nashville, TN 37232, USA. [4]Department of Biological Sciences, University of Pittsburgh, Pittsburgh, PA 15260, USA.

*Author for correspondence (plageman.3@osu.edu)

Received 2 January 2014; Accepted 5 June 2014

Conventionally, AC was thought to depend on apical circumferential actomyosin contraction that reduces the apical area in a drawstring-like mechanism. Recent work in invertebrates, however, has demonstrated that AC is driven by a network of actomyosin filaments spanning the apical cortex that contract in pulses rather than in a continuous smooth motion (Martin et al., 2009; Solon et al., 2009; David et al., 2010; Mason et al., 2013). The actomyosin filaments are associated with the zonula adherens (ZA), which are the adherens junctions of epithelial cells, and upon contraction apply an inward pulling force to the junctional complex. Actomyosin contraction in both *Caenorhabditis elegans* and *Drosophila* initiates prior to AC and the reduction of the apical area occurs only after the contractile filaments are engaged with cell contact zones (Roh-Johnson et al., 2012). A current challenge is to determine whether these mechanisms are conserved in vertebrates and to identify the molecules responsible for linking apical junctions with the AC machinery.

Although it is unclear whether apical actomyosin filaments drive AC in vertebrates, ZA proteins have been implicated. In *Xenopus*, morpholinos directed toward *N-cadherin* or *nectin-2* result in a failure of AC and neural tube closure due to the lack of F-actin filament assembly (Nandadasa et al., 2009; Morita et al., 2010). Similarly, the loss of several F-actin assembly proteins known to associate with the ZA also causes neurulation and/or gastrulation defects in vertebrates (Koleske et al., 1998; Xu et al., 1998; Iioka et al., 2004; Roffers-Agarwal et al., 2008). Whether any of these F-actin assembly proteins in vertebrates facilitates the engagement of actomyosin filaments with the ZA during AC has yet to be determined. The cadherin-binding ZA protein p120-catenin (also known as delta1 catenin) directly affects the cytoskeleton through the modulation of GTPases, which are crucial regulators of actin dynamics and AC (Pieters et al., 2012). Although severe morphogenetic defects occur in the absence of p120-catenin in vertebrates (McCrea and Park, 2007), its role in AC has yet to be tested.

Lens placode invagination has previously served as an informative model for AC during vertebrate embryonic morphogenesis (Plageman et al., 2010, 2011b; Chauhan et al., 2011). Through this work we have detailed the role of Shroom3, a cytoskeletal protein that directs Rho kinase- and RhoA-dependent AC in the lens placode and partially facilitates invagination (Plageman et al., 2010, 2011b). In this study, we utilized lens placode invagination to probe the relationship between Shroom3-dependent AC and the ZA. We found that, similar to invertebrate AC, contractile myosin filaments spanning the apical cortex and anchored at the ZA are also present in vertebrate apically constricting cells. We demonstrate that among several ZA proteins Shroom3 preferentially genetically interacts with p120-catenin and, like Shroom3, p120 is required for lens pit AC and apical myosin localization. Furthermore, we demonstrated that p120-catenin plays a key role in recruiting Shroom3 to the ZA. Together, these data reveal the importance of the ZA and p120-catenin to Shroom3-dependent AC.

Development (2014) 141, 3177-3187 doi:10.1242/dev.107433

RESULTS

Apical cortex-spanning myosin filaments in apically constricting vertebrate cells

Invertebrate apically constricting cells depend on an apically positioned network of non-muscle myosin, which contracts in pulses. To determine whether vertebrate cells have a similar network, localization of non-muscle myosin IIb and F-actin was examined in apically constricting cells of E10.0 mouse embryo lens placodes. The apical junctions of lens placodal cells have intense myosin IIb and F-actin (Fig. 1A-C) labeling that colocalizes with the prominent ZA protein β-catenin, although higher magnification revealed that myosin IIb and F-actin are also localized to apically positioned filament-like structures spanning the apical cortex, which are β-catenin negative (Fig. 1C,F-H). *z*-projections and images taken 2 µm below the apical surface confirm that these actomyosin filaments are apically positioned (Fig. 1F-H). Placodal cells contain one or several actomyosin filaments and, in the latter case, they are orientated in approximately the same direction (Fig. 1C). Directionally marking all actomyosin filament-containing cells within a lens placode (defined by a dashed line marking the area adjacent to the underlying optic vesicle, Fig. 1A,B) revealed that they are generally arranged in a tangential pattern, preferentially located in the periphery (Fig. 1D), and the average angle of the filaments is close to perpendicular with respect to the radius [91.3±3.06° (s.e.m.)]. Additionally, the average apical area of the central lens placodal cells is significantly smaller than that of the peripheral placode (Fig. 1E), demonstrating that the timing of AC between the two cell populations differs. Placodal cells with prominent actomyosin filaments also have larger apical areas in both the central and peripheral regions (Fig. 1E). Although not conclusive, these data are consistent with the possibility that actomyosin filaments form prior to AC and possibly disassemble once the apical area has been reduced.

The actomyosin filaments are anchored to both tricellular and bicellular junctions and, in the latter case, are coincident with local deformations of the junction, suggesting that the filament is under

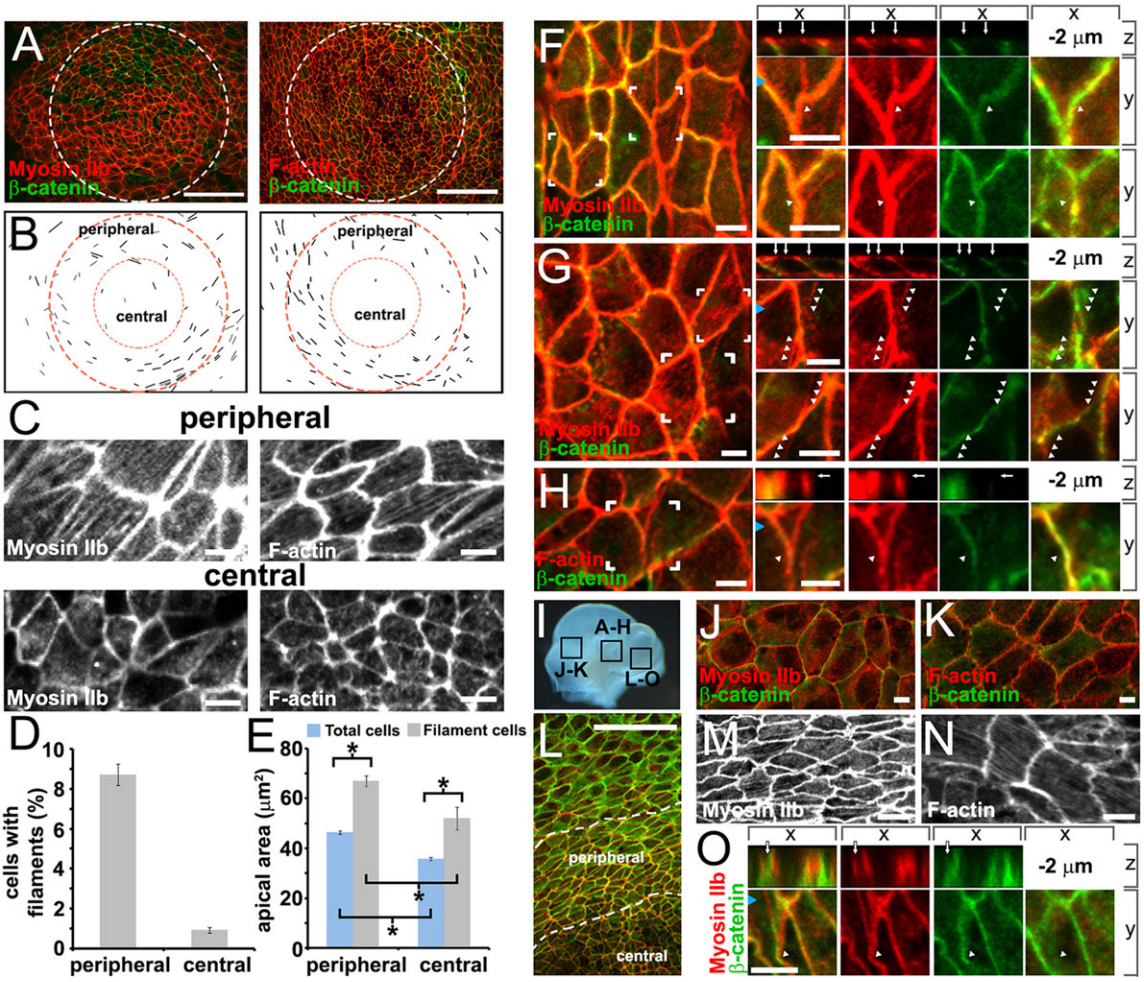

Fig. 1. Myosin IIb filaments span the apical domain of apically constricting cells of the lens placode. (A) *En face* view of whole-mount E10.0 mouse lens placode colabeled for β-catenin and myosin IIb or F-actin. The white dashed line indicates the region of the lens placode. (B) Prominent actomyosin filaments in A that do not colocalize with junctions and that span the apical surface of cells were traced with black lines. The radius of the central lens placode region is half that of the outer peripheral boundary. (C) Higher magnification of representative regions from lens placodes fluorescently labeled for myosin IIb or F-actin. (D,E) The average percentage of cells with actomyosin filaments in the central or peripheral region (n=5) (D) and the average apical area of all cells from three placodes (E). Error bars indicate s.e.m.; *P<0.05. (F-H) *En face* view of lens placodes at the level of apical junctions, with magnification of the bracketed regions shown to the right. The far right panel is an image taken 2 µm below the apical junctions. White arrowheads demarcate fibers associated with apical junctions that appear to be under tension (F,H) or fibers that appear to traverse the junctions (G). White arrows indicate the apical position of the fibers. (I) Approximate positions of the E10.0 *en face* images shown in the panels indicated. (J,K) *En face* view of head ectoderm. (L-O) *En face* view of nasal placode. Scale bars: 50 µm in A; 5 µm in C,F-K,M-O; 20 µm in L.

Development (2014) 141, 3177-3187 doi:10.1242/dev.107433

tension (arrowheads in Fig. 1F,H). They also often appear to align themselves with others from neighboring cells and can span up to three to four cell lengths in an almost straight line (arrowheads, Fig. 1G). A more intense β-catenin signal at the filament intersection is also observed (Fig. 1G). These filaments are not usually found in the non-apically constricting cells of the head ectoderm (Fig. 1J,K), but are observed in cells within the periphery of the invaginating nasal placode (Fig. 1L-N) and are coincident with junctional displacement (Fig. 1O).

To determine whether these actomyosin filaments are contractile, E10.0 mouse embryos were cultured for 90 min in the presence or absence of the myosin II inhibitor Blebbistatin or of Calyculin A, a phosphatase inhibitor known to activate myosin II activity (Somlyo and Somlyo, 2000). Subsequently, the embryos were fixed, immunofluorescently labeled for myosin IIb and β-catenin, and the bicellular junctional displacement of placodal cells was measured (Fig. 2A). As expected, embryos cultured in the absence of inhibitors have bicellular junctions associated with filaments that appear curved and displaced, and on average the displacement was significantly greater than the width of the β-catenin labeling of a straight bicellular junction (Fig. 2B,F). By contrast, Blebbistatin-treated embryos have junctions that are not locally deformed (Fig. 2C,F), which is indicative of a reduction in force applied to the junctions at the point of filament contact. Similar to the control embryos, Calyculin A-treated embryos had displaced bicellular junctions, and on average the displacement was not significantly greater than normal (Fig. 2D,F). However, we observed that in patches of cells this displacement appeared exaggerated and the junctional β-catenin signal did not colocalize with myosin IIb (Fig. 2E). *z*-projection reveals that junctional myosin appears to have pulled away from junctional β-catenin (Fig. 2E, top row). In extreme cases, the myosin signal was fully pulled away from the junctions and contracted into a ring devoid of structure (Fig. 2E, bottom row). In addition, the proportion of cells with filaments was increased with Calyculin A treatment, whereas Blebbistatin-treated embryos had fewer filament-containing cells and those that did had a larger apical area (Fig. 2G). Because the displacement of junctions is correlated with myosin activity, these data strongly suggest that the observed filaments are contractile, and this contraction is myosin dependent. Importantly, these data are also consistent with the idea that myosin activity is not sufficient for junctional displacement or AC, implicating a requirement for additional factors.

Shroom3 functions cooperatively with p120-catenin

Given that Shroom3, a protein necessary and sufficient for AC, localizes to adherens junctions in epithelia, a genetic interaction screen was performed to identify ZA proteins that may function with Shroom3. Heterozygous *Shroom3* mice (*Shroom3*$^{+/Gt}$) that also express Cre recombinase in the Shroom3 expression domain (Hildebrand and Soriano, 1999) were crossed with homozygous mice carrying floxed alleles of the ZA genes E-cadherin [*E-cad*; also known as cadherin 1 (*Cdh1*)], N-cadherin [*N-cad*; also known as cadherin 2 (*Cdh2*)], β-catenin (*β-cat*; *Ctnnb1* – Mouse Genome Informatics) and p120-catenin (*p120*; also known as *Ctnnd1*).

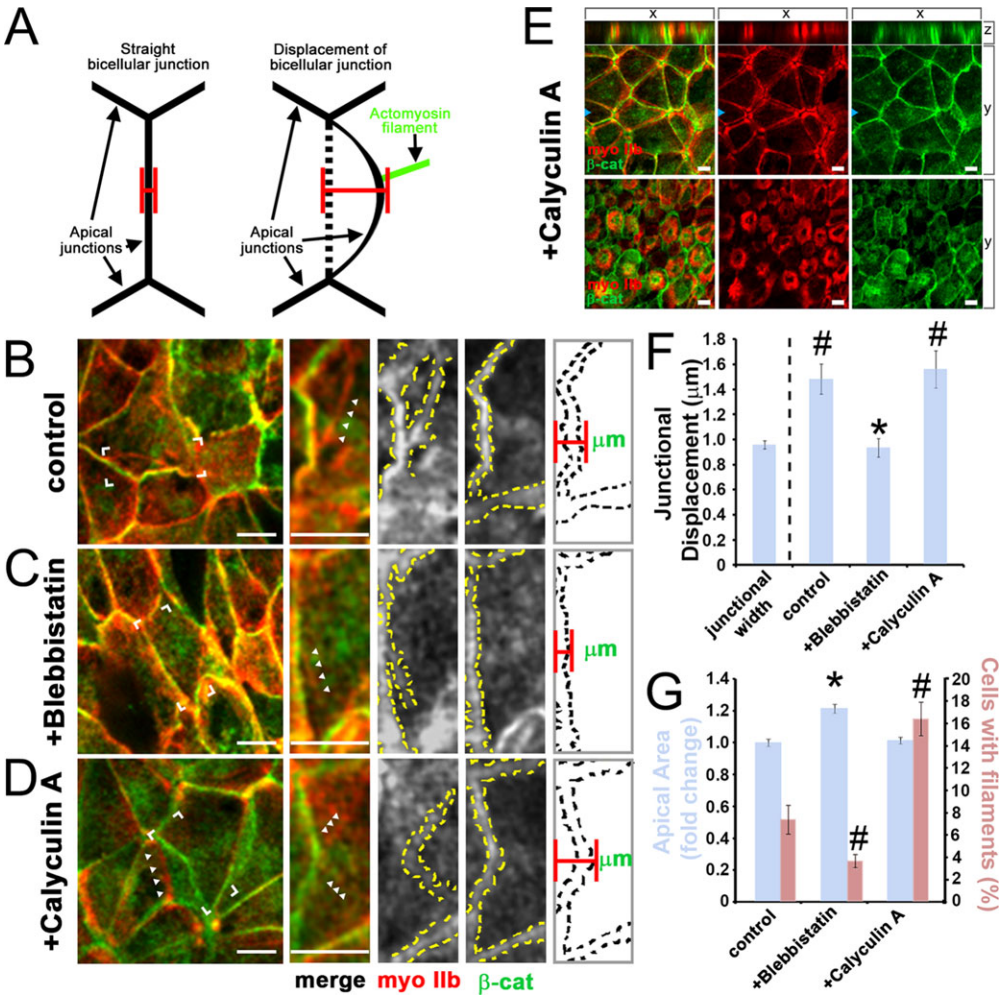

Fig. 2. Apical myosin IIb filaments are contractile. (A) Schematic detailing how bicellular junction displacement is measured. Red brackets indicate the measured dimension. (B-D) *En face* view of whole-mount E10.0 embryos cultured in control media (B) or media containing Blebbistatin (C) or Calyculin A (D). Immunostaining is for myosin IIb (red) and β-catenin (green). The bracketed regions are magnified to the right. Arrowheads indicate myosin filaments and the dashed lines outline the junctional and/or the myosin filament signal. (E) Representative *en face* and *z*-projection (top row) images of Calyculin A-treated placodes immunolabeled as indicated. Note the separation from myosin signal from the junctions. (F) Average width of β-catenin-labeled junctions and the distance of junctional displacement. (G) Average fold change in apical areas measured using boundaries determined from junctional labeling, and the average number of cells with filaments. Error bars indicate s.e.m.; **P*<0.05 versus control and $^{\#}$*P*<0.05 versus filament-nonassociated junctional width. Scale bars: 5 μm.

Development (2014) 141, 3177-3187 doi:10.1242/dev.107433

Pregnant dams were euthanized from E9.5-15.5 and the embryos were analyzed for neural tube or ocular defects, both of which are phenotypes found in 100% of *Shroom3*$^{Gt/Gt}$ embryos (Table 1, Fig. 3B,F,J). Because heterozygous embryos lacking one copy of *Shroom3*, E-cadherin, N-cadherin or p120-catenin are reported not to have neural tube or ocular defects (Radice et al., 1997; Hildebrand and Soriano, 1999; Huelsken et al., 2000; Boussadia et al., 2002; Davis and Reynolds, 2006), a doubly heterozygous embryo with a neural tube phenotype or ocular abnormality would indicate a genetic interaction with *Shroom3*.

As expected, all control embryos heterozygous for a floxed allele and homozygous for the wild-type *Shroom3* allele did not have neural tube or ocular defects and appeared phenotypically normal (Table 1, Fig. 3A,E,I). Similarly, neither *Shroom3*$^{+/Gt}$; *E-cad*$^{+/flox}$ nor *Shroom3*$^{+/Gt}$; *β-cat*$^{+/flox}$ embryos consistently displayed an abnormal phenotype (Table 1). We previously reported that *Shroom3*$^{+/Gt}$; *N-cad*$^{+/flox}$ embryos have neural tube defects at a low but consistent rate (Table 1, Fig. 3C,G) (Plageman et al., 2011a). At E12.5 these embryos also have ocular defects in which the retinal pigmented epithelium covers a greater area of the dorsal eye in a manner similar to *Shroom3* mutant embryos (Fig. 3J,K). By contrast, a large majority of *Shroom3*$^{+/Gt}$; *p120*$^{+/flox}$ embryos have neural tube and ocular defects that are strikingly similar to those of *Shroom3*$^{Gt/Gt}$ embryos (Table 1, Fig. 3D,H,L), indicating that of the ZA genes analyzed, a strong genetic interaction with Shroom3 occurs most readily with p120-catenin, suggesting that their gene products are functioning together during morphogenesis.

p120-catenin is required for Shroom3-dependent AC

Because of the strong *p120*/*Shroom3* genetic interaction, we next determined whether conditional p120-catenin deletion, like germline deletion of Shroom3, disrupts lens pit invagination. The course of normal lens pit invagination can conceptually be broken down into five stages (Fig. 4A), where the first stage is defined as a lens placode with the first hint of inward bending. During the second and third stages the lens cells elongate and the curvature of the lens placode extends to a shallow arc (stage II), and then to a semicircular shape (stage III). An omega-shaped lens pit forms in the fourth stage due to the formation of hinge points (white arrowheads, Fig. 4A) that appear radially near the surface ectoderm and drive the process of lens pit closure, which occurs at stage V.

Upon deletion of p120-catenin utilizing the *AP2α-cre* line [AP2α (Tfap2a) is expressed in structures derived from the head ectoderm and surrounding mesenchyme (Macatee et al., 2003)], the progression of lens pit invagination shows the earliest sign of malformation at stage III and the lens pit has relatively straight epithelia without curvature at the lateral margins (white lines, Fig. 4A). A comparison

Table 1. The percentage of embryos of the indicated genotypes that exhibit severe morphological defects as defined by neural tube or ocular malformations

Genotype	Number	Percentage
Shroom3$^{+/Gt}$	0/54	0
Shroom3$^{+/+}$; *E-cad*$^{+/flox}$	0/13	0
Shroom3$^{+/+}$; *N-cad*$^{+/flox}$	0/21	0
Shroom3$^{+/+}$; *β-cat*$^{+/flox}$	0/11	0
Shroom3$^{+/+}$; *p120*$^{+/flox}$	0/57	0
Shroom3$^{Gt/Gt}$	25/25	100
Shroom3$^{+/Gt}$; *E-cad*$^{+/flox}$	0/10	0
Shroom3$^{+/Gt}$; *N-cad*$^{+/flox}$	5/19	26.3
Shroom3$^{+/Gt}$; *β-cat*$^{+/flox}$	1/8	12.5
Shroom3$^{+/Gt}$; *p120*$^{+/flox}$	44/52	84.6

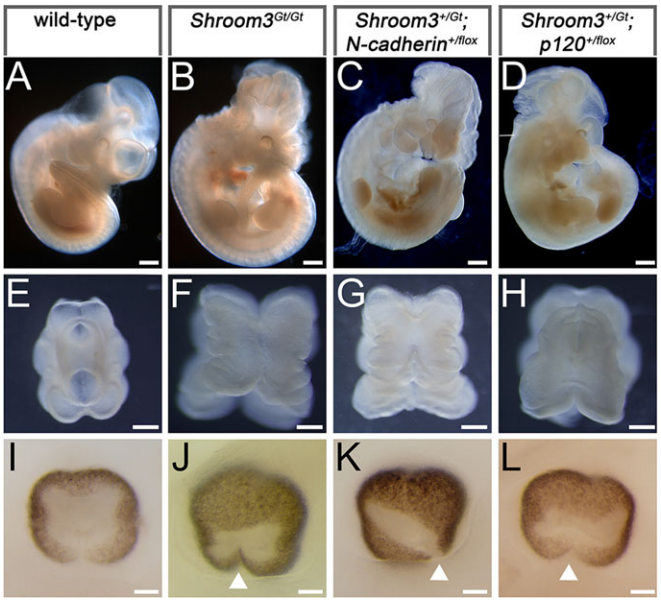

Fig. 3. Shroom3 genetically interacts with p120-catenin. (A-H) Representative images of whole E10.75 mouse embryos (A-D) and anterior views of E10.75 mouse heads (E-H) of the indicated genotypes. (I-L) Representative images of the eye from E12.5 mouse embryos. Arrowheads indicate the location of ventral optic cup abnormalities. Scale bars: 500 µm in A-H; 125 µm in I-L.

with Shroom3-deficient embryos demonstrates that the shape of the lens pit is similar and their lens pits similarly lack hinge points at stages IV and V (white arrows, Fig. 4A). However, the lateral lens pit epithelia appear without curvature one stage earlier in the *Shroom3* mutants than in the p120-catenin mutants.

To quantify differences in lens pit shape, the average *x-y* coordinates of the outer (basal) and inner (apical) margins of stage III lens pits were determined and curvature values were calculated for each apical coordinate (Fig. 4B; supplementary material Fig. S1). Curvature was significantly decreased in the lateral but not the central lens pit of p120-catenin-depleted and Shroom3-depleted embryos (Fig. 4C). p120-catenin is likely to affect the lens pit epithelium directly, as mesenchymal depletion of p120-catenin does not affect hinge point formation or cause a change in lens pit morphology (supplementary material Fig. S2).

To determine if AC is inhibited in p120-catenin-deficient embryos, the width at seven equally spaced positions along the apicobasal axis and the height of all individual lens pit cells from central cryosections of stage III embryo lenses were measured based on the junctional signal from immunolabeling with an antibody specific for β-catenin. On average, the cells in p120-catenin-deficient stage III lens pit are significantly wider at the four apicalmost points and shorter than those of *p120*$^{flox/flox}$ embryos (Fig. 4D,E). Comparing these data with width and height data from a previous analysis of *Shroom3*$^{Gt/Gt}$ mutant embryos (Plageman et al., 2010) reveals a similar pattern of wider and shorter cells and that their average shapes are remarkably similar (Fig. 4D,E). Hinge point formation in the lens pits of *Shroom3*$^{Gt/Gt}$ results in an elongated lens pit that does not completely pinch off from the surface ectoderm, and at E15.5 the lens vesicle is reduced in size and remains connected to the future cornea (Fig. 4A, E15.5). Although *AP2α-cre*; p120$^{flox/flox}$ embryos have similar elongated lens pits and lack hinge points at stages IV and V (Fig. 4A, arrows), the lens pits pinched off in all embryos examined. However, one abnormality observed was the absence of the gap that is normally present between the lens vesicle and ocular mesenchyme, which is consistent with the

Development (2014) 141, 3177-3187 doi:10.1242/dev.107433

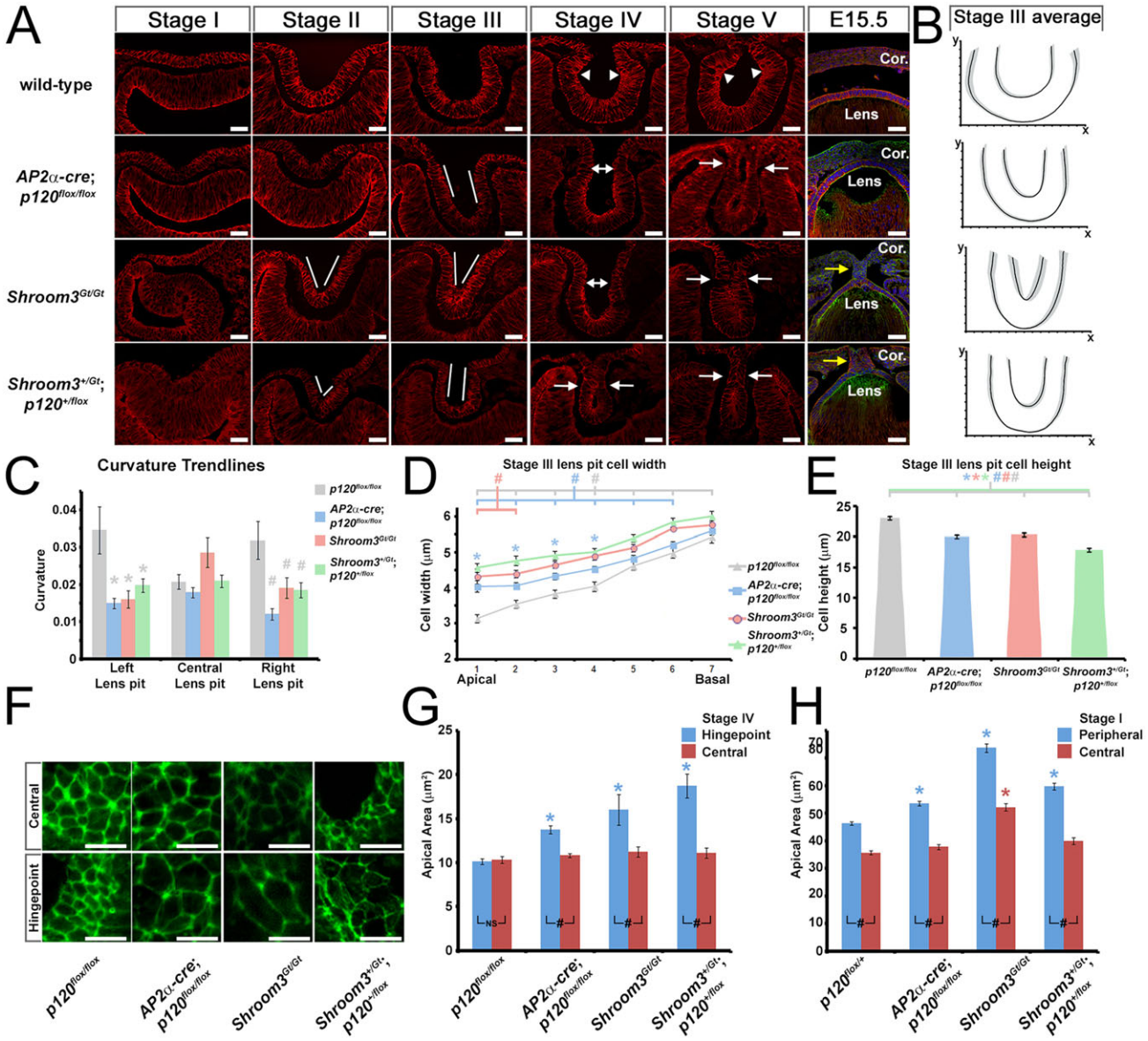

Fig. 4. Shroom3 or p120 deficiency similarly disrupts lens pit invagination. (A) Cryosections from mouse embryo lenses during lens pit invagination (E10.0-10.75) and at E15.5. Sections were fluorescently labeled for β-catenin (red) alone (stages I-IV) or with F-actin (green) and Hoechst (blue) (E15.5). Scale bars: 25 μm, except 50 μm for E15.5. The white lines mark a straight epithelial shape; arrowheads indicate lens pit hinge points, whereas white arrows indicate their absence. Yellow arrows point to the lack of cornea (Cor.) and lens separation. (B) Average (*x*,*y*) coordinates (black line) for the apical and basal boundary of lens pits. The flanking gray area represents the average (*x*,*y*) coordinate plus or minus the s.e.m. (C) Average apical curvature values for the central or lateral regions of the lens pit calculated from the (*x*,*y*) coordinates determined for B. (D) Comparison of stage III lens pit cell width. **P*<0.05 for *p120*$^{flox/flox}$ versus *Ap2α-cre*; *p120*$^{flox/flox}$; $^{\#}$*P*<0.05 for *p120*$^{flox/flox}$, *AP2a-cre*; *p120*$^{flox/flox}$ or *Shroom3*$^{Gt/Gt}$ versus *Shroom3*$^{+/Gt}$; *p120*$^{+/flox}$. (E) Comparison of stage III lens pit cell height. The width of the bars is also representative of the average cell width along the apicobasal axis based on the data in D and is proportional to the cell height. (F) Non-central cryosections of stage IV lens pits in the central and hinge point regions where the apical surface is exposed for multiple cells fluorescently labeled for F-actin. Scale bars: 5 μm. (G,H) Average apical area based on immunolabeling of stage IV lens pit cryosections or *en face* images of stage I placodes. (C,E,G,H) **P*<0.05; $^{\#}$*P*<0.05 compared with the appropriate control genotype. Error bars indicate s.e.m.

findings of another study in which p120-catenin was depleted specifically in the ocular mesenchyme (Tian et al., 2012).

Analysis of doubly heterozygous *Shroom3*$^{+/Gt}$; *p120*$^{+/flox}$ embryos revealed that, like *Shroom3*$^{Gt/Gt}$ mutants, their lateral lens pit epithelia at stage II-III exhibit quantitatively less curvature, at later stages fail to develop hinge points, and at E15.5 the lens vesicle remains attached to the cornea (Fig. 4A-C). Quantitative assessment of doubly heterozygous *Shroom3*$^{+/Gt}$; *p120*$^{+/flox}$ stage III lens pit cell shapes surprisingly revealed that the cells are significantly wider at the apex and shorter than those of any of the other three genotypes analyzed (Fig. 4D,E). The exacerbated phenotype is also consistent with the observation that, unlike *Shroom3*$^{Gt/Gt}$ or *AP2α-cre*; p120$^{flox/flox}$ embryos, *Shroom3*$^{+/Gt}$; *p120*$^{+/flox}$ embryos sometimes do not have a lens pit at E10.5, possibly owing to a complete failure in lens pit invagination (data not shown; *n*=3). To determine whether the failure in hinge point formation is due to a failure in regional AC of later lens pits, the apical surface of stage IV lens pit cells was examined. In control embryos the average apical areas of hinge point and central cells are approximately the same, whereas the apical area of lateral lens pit

Development (2014) 141, 3177-3187 doi:10.1242/dev.107433

cells is significantly larger than that of central cells in mutant embryos (Fig. 4F,G), indicating that the hinge point region is selectively affected. This regionally restricted cell shape phenotype is consistent with a localized increase in the apical area of peripheral stage I lens placodal cells in mutant embryos (Fig. 4H). The regional susceptibility to perturbations in cell shape suggests that p120-catenin function is particularly important for peripheral/hinge-point cell AC.

Both p120-catenin and Shroom3 appear to localize mostly to the ZA and do not appear to strongly colocalize with prominent actomyosin filaments that span the apical cortex (supplementary material Fig. S3; Fig. 5C-I). Because Shroom3-deficient and p120-catenin-deficient embryos have a reduction in AC, we next asked whether bicellular junctional displacement at the point of myosin IIb filament association is altered. Not surprisingly, wild-type (*Shroom3*$^{+/+}$; *p120*$^{+/flox}$) embryos have locally displaced bicellular junctions (Fig. 5A) and, when quantified, the displacement is significantly greater than the width of a straight filament-nonassociated junction (Fig. 5B). By contrast, mutant embryos lacking Shroom3 and/or p120-catenin have filament-associated bicellular junctions that do not curve and on average are not significantly displaced (Fig. 5B). The paucity of displaced junctions in the mutant embryos is consistent with the idea that AC is inhibited by a disruption of the contractile myosin filaments and the components of the ZA.

To further probe why p120-catenin deficiency leads to a failure in AC, the localization of p120-catenin, Shroom3, non-muscle myosin and F-actin was analyzed in histological sections of lens pits of mutant embryos. In *AP2α-cre*; *p120*$^{flox/flox}$ embryos, but not *Shroom3*$^{+/Gt}$; *p120*$^{+/flox}$ embryos, p120-catenin is expectedly absent from the lens pit (Fig. 5C-E). Quantitative assessment of fluorescence intensity across lens pit cellular junctions confirmed this observation (Fig. 5F). The fold increase in p120-catenin intensity across junctions compared with neighboring cytoplasmic signal was not reduced in p120-catenin heterozygotes suggesting that the p120 catenin protein that is generated is properly localized. However, calculating the average peak p120-catenin intensity revealed a 27.4% decrease in lens cell junctions compared with control cells, indicating an overall decrease in protein levels. Shroom3 (Fig. 5G-J) and myosin IIb (Fig. 5K-N) are quantifiably reduced in the apical junctions of hinge point cells in the absence of

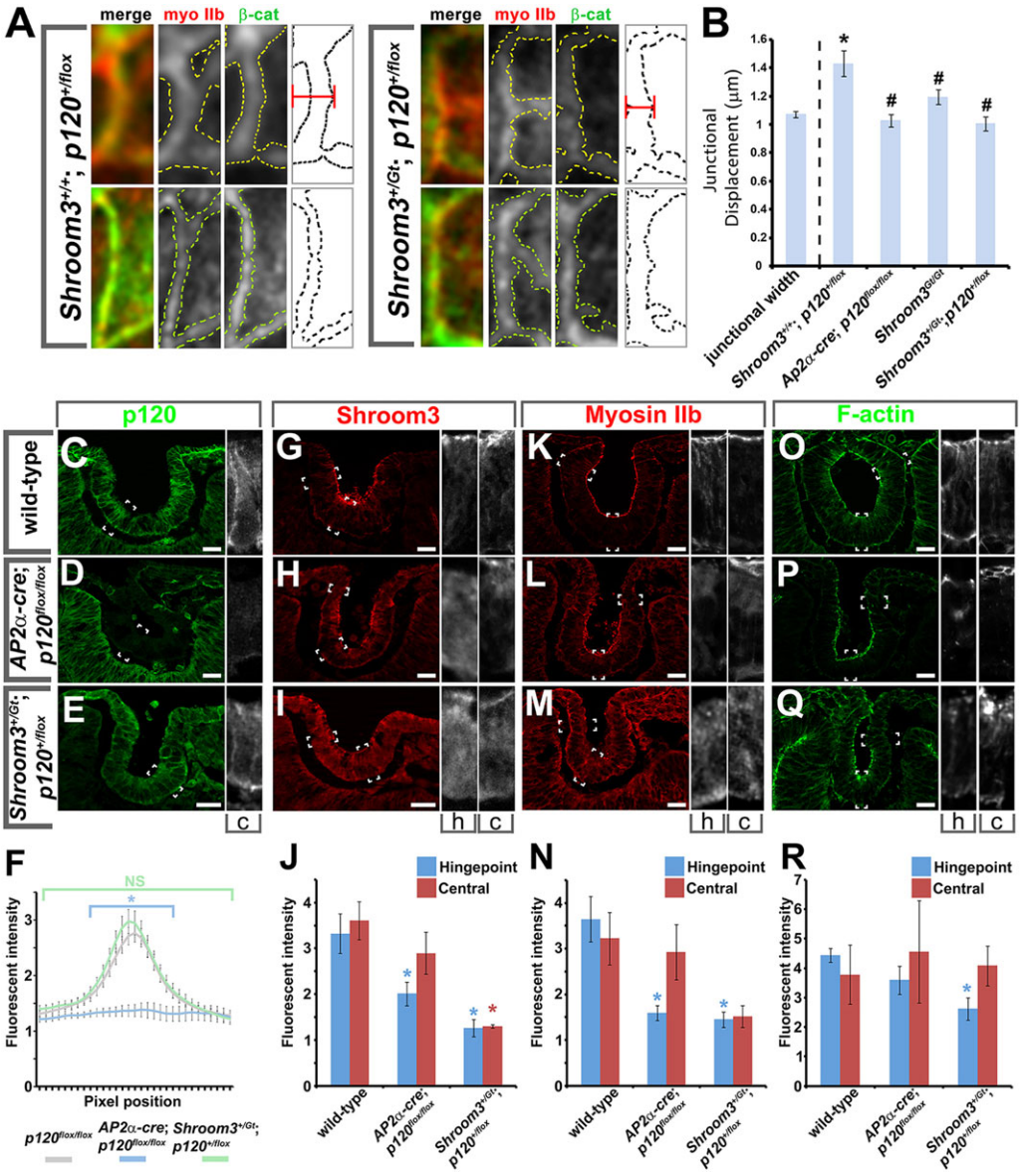

Fig. 5. Junctional displacement inhibition and mislocalization of myosin IIb/Shroom3 in p120-catenin-deficient lens pits. (A) Magnified *en face* view of lens placode bicellular junctions associated with myosin filaments. Dashed lines indicate the localization of the junctional and/or apically positioned filaments. (B) Comparison of the average junctional displacement. **P*<0.05 versus junctional width of a filament-nonassociated bicellular junction; #*P*<0.05 versus control genotype. (C-Q) Cryosections of mouse embryo lenses immunolabeled with antibodies specific to p120-catenin (C-E), Shroom3 (G-I), myosin IIb (K-M) or phalloidin to label F-actin (O-Q). The central (c) or upper hinge point (h) regions are magnified from the bracketed areas. (F) The average intensity of p120-catenin signal along a straight line drawn across apical junctions. NS, not significant. (J,N,R) The average apical signal of Shroom3 (J), myosin IIb (N) and F-actin (R) of the central or hinge point regions. **P*<0.05 versus wild type. Error bars indicate s.e.m. Scale bars: 25 μm.

Development (2014) 141, 3177-3187 doi:10.1242/dev.107433

p120-catenin, but apical localization in the central portion of the lens pit is unchanged. The doubly heterozygous *Shroom3*$^{+/Gt}$; *p120*$^{+/flox}$ embryos have a significant reduction in both hinge point and central cells, with the exception of myosin IIb localization in the central cells, which is lower but not significantly so (Fig. 5G-N). By contrast, F-actin does not appear to be significantly affected, except in hinge point cells of the doubly heterozygous embryos (Fig. 5O-R). These data are indicative of a role for p120-catenin in directing the apical localization of both Shroom3 and myosin IIb, specifically within the hinge point cells.

The loss of apical Shroom3 recruitment in the absence of p120-catenin and the *in vivo* AC phenotype of p120-catenin-deficient lens pits prompted further investigation into whether p120-catenin is required for Shroom3 function. MDCK cells that are depleted of p120-catenin by RNAi were generated (Fig. 6A,B). ZO-1 (Tjp1) labeling revealed that, in the absence of p120-catenin, the cells still form tight junctions (Fig. 6C,D), similar to previous findings (Dohn et al., 2009). Unlike wild-type MDCK cells, when Shroom3 is transiently expressed in p120-catenin-deficient cells, apical area is not reduced compared with Shroom3 non-expressing cells (Fig. 6E-G). p120-catenin deficiency also causes a general increase in cell size (Fig. 6C,D), possibly owing to a general relaxation of cytoskeletal elements.

To determine if the failure of Shroom3 to induce AC is due to a lack of junctional recruitment, Shroom3 was transiently expressed with wild-type N-cadherin (N-cadherin^{wt}) (Fig. 6H,I) or with mutant N-cadherin that cannot bind to p120-catenin (N-cadherin^{AAA}) (Fig. 6J,K). Shroom3-induced AC occurs to a similar degree with or without the co-expression of wild-type N-cadherin, but in the presence of mutant N-cadherin Shroom3 does not induce AC (Fig. 6J,K) and the average apical:basal area ratio is close to 1 (Fig. 6L). These data demonstrate that not only is p120-catenin required for Shroom3-induced AC but also that Shroom3 function requires junctional p120-catenin.

p120-catenin recruits Shroom3 to the ZA

Although overexpression of mutant N-cadherin inhibited Shroom3-induced AC, exogenous Shroom3 still appeared to localize junctionally (Fig. 6K). A possible explanation is the presence of endogenous cadherin proteins not involved in AC (such as E-cadherin) that still bind to p120-catenin and recruit Shroom3. To overcome the confounding presence of additional cadherins N-cadherin^{wt} or N-cadherin^{AAA} was ectopically expressed in A431D cells, which normally do not express endogenous cadherins. Transgenic A431D cells expressing N-cadherin^{wt} effectively recruit p120-catenin to adherens junctions (Fig. 7A), whereas N-cadherin^{AAA}-expressing cells do not (Fig. 7D). The degree to which p120-catenin is recruited was also quantified by measuring the signal intensity along a short line drawn perpendicular to the junctions on images taken of immunofluorescently labeled cells, and no signal peak of p120-catenin labeling was detected at the junction of cells expressing N-cadherin^{AAA} (Fig. 7F). To determine if Shroom3 was similarly affected, it was expressed in A431D cells expressing N-cadherin^{wt} or N-cadherin^{AAA}. Significantly less Shroom3 is localized to the junctions of N-cadherin^{AAA}-expressing cells (Fig. 7E,G) compared with N-cadherin^{wt}-expressing cells (Fig. 7B,G), indicating that the p120-catenin-binding domain of N-cadherin is required to effectively recruit Shroom3 to adherens junctions.

It was recently reported that p120-catenin also mediates the recruitment of Rock to adherens junction (Smith et al., 2012). Because Shroom3 binds to Rock (Mohan et al., 2012) we determined whether p120-catenin recruits Shroom3 via Rock binding. To block Rock binding to Shroom3, a single missense

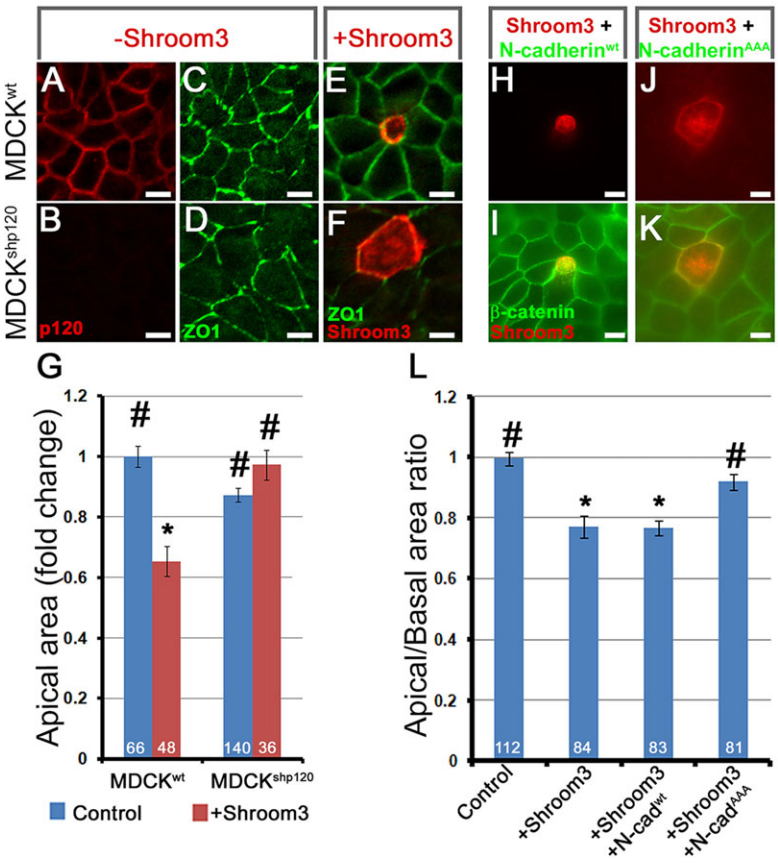

Fig. 6. Junctional p120-catenin is required for Shroom3-induced AC. (A-F) Control (MDCK^{wt}) or p120-catenin-deficient (MDCK^{shp120}) MDCK cells transiently transfected with Shroom3 and immunolabeled for p120-catenin (A,B), ZO-1 (C,D) or Shroom3 and ZO-1 (E,F). (G) Apical area comparison of control and Shroom3^{+} MDCK^{wt} or MDCK^{shp120} cells. **P*<0.05 versus control MDCK^{wt} cells; $^{\#}$*P*<0.05 versus Shroom3^{+} MDCK^{wt} cells. (H-K) Shroom3^{+} and N-cadherin^{wt+} or N-cadherin^{AAA+} MDCK cells immunolabeled for Shroom3 (red) and β-catenin (green). (L) Average apical:basal area ratios of transfected MDCK cells. **P*<0.05 versus non-transgenic MDCK cells; $^{\#}$*P*<0.05 versus Shroom3/N-cadherin^{wt}-expressing cells. Error bars indicate s.e.m. The number of cells measured is indicated. Scale bars: 15 µm.

Development (2014) 141, 3177-3187 doi:10.1242/dev.107433

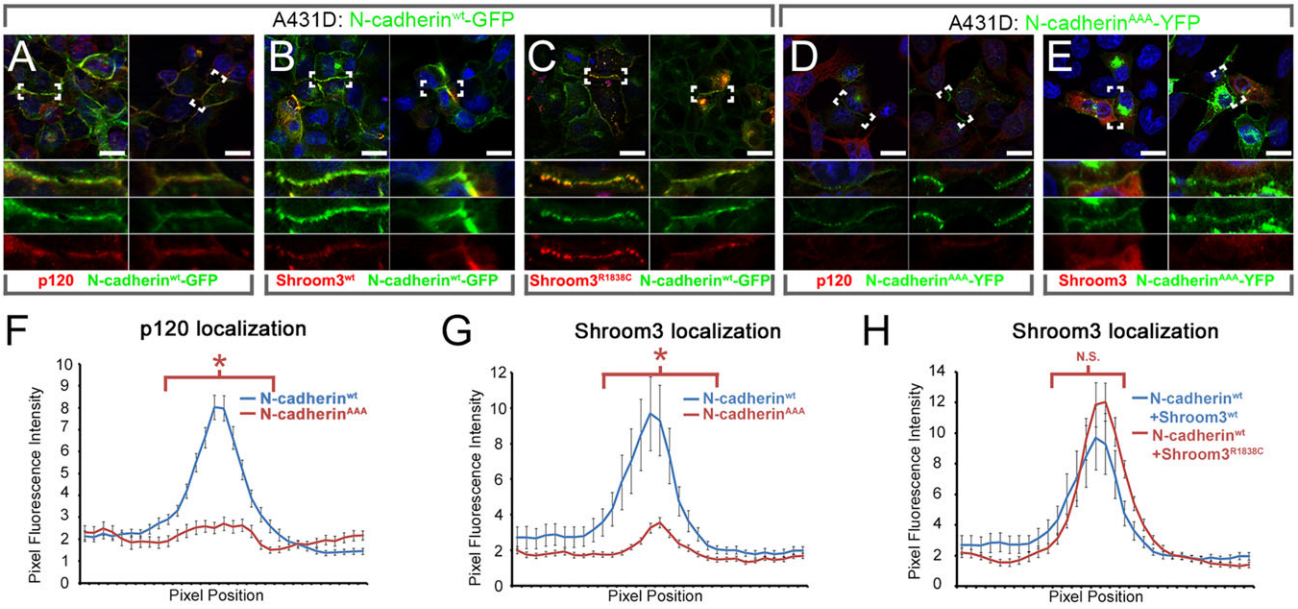

Fig. 7. Shroom3 junctional localization is facilitated by p120 catenin. (A-E) Stable transgenic lines of endogenous cadherin-deficient A431D cells expressing N-cadherin^{wt} (A-C) or p120-catenin binding-deficient N-cadherin^{AAA} (D,E) transiently transfected with Shroom3 (B,E) or the Rock binding-deficient Shroom3 mutant (Shroom3^{R1838C}) (C) immunolabeled for p120-catenin (red) (A,D) or Shroom3 (red) (B,C,E). The bracketed junctions are magnified in the panels beneath. (F-H) Comparison of the average fluorescence intensity values for p120-catenin (F) or Shroom3 (G,H) along line intervals perpendicular to the cell junctions. Error bars indicate s.e.m.; *P<0.05 versus wild-type construct for the bracketed data points. N.S., not significant. Scale bars: 20 µm.

mutation was generated (Shroom3^{R1838C}) that lies within a short critical sequence known to associate with Rock1 (Mohan et al., 2012). Furthermore, this exact same missense mutation causes severe morphogenetic defects that are similar to those found in mice with a germline deletion of *Shroom3* (Marean et al., 2011; Massarwa and Niswander, 2013). When Shroom3^{R1838C} was expressed in A431D cells that express N-cadherin^{wt}, it was effectively recruited to the junctions (Fig. 7C) and the junctional signal was not significantly lower than with Shroom3^{wt} (Fig. 7H). This result indicates that although p120-catenin recruits Shroom3 it does not do so indirectly through Rock binding.

DISCUSSION

Cellular organization of cytoskeletal proteins necessary for AC

One of the unresolved questions concerning vertebrate AC is whether it is driven by apical cortex-spanning actomyosin filaments, similar to the process in invertebrates (Martin et al., 2009; Solon et al., 2009; David et al., 2010; Mason et al., 2013). Much like apical constricting cells in *Drosophila*, mouse lens placodal cells have actomyosin filaments that span apical junctions within 2 µm of the apical surface. Notably, bicellular junctions are deformed at the anchor point between the non-muscle-myosin-containing filaments and apical junctions and the deformation is dependent on non-muscle myosin activity, Shroom3 and p120-catenin. These structures were also found exclusively within invaginating tissues (lens and nasal placode) and not generally throughout the head ectoderm. The localization of filaments in cells found in the periphery of the lens placode and their tangential directionality hint that AC might occur anisotropically and/or might be regulated by planar cell polarity pathways. These possibilities are consistent with anisotropic AC and planar polarization of Shroom3 pathway proteins in *Drosophila* (Martin et al., 2010; Simoes Sde et al., 2014).

A significant difference between apically constricting lens placodal cells and *Drosophila* mesodermal cells is the lack of strong junctional localization in the latter (Martin et al., 2009). The architecture of apical myosin also appears morphologically distinct and is arranged as a multidirectional network of spots and filaments in *Drosophila*, whereas the filaments are prominently unidirectional in the mouse lens (Martin et al., 2009). We do observe an apical, diffuse pattern of myosin, F-actin and Shroom3 staining without identifiable structure but the purpose of the proteins with this localization is not obvious in our fixed tissue samples. Without real-time monitoring of the nature of these filaments we have not definitively demonstrated that medial contractions of actomyosin rather than junctional actomyosin actively reduce the apical area of lens placodal cells. It remains possible that the main driving force of AC in the lens placode is due to contraction of junctional actomyosin. However, the cortex-spanning filaments are contractile and specific to lens placodal cells with larger apical areas and are more prevalent in the periphery, suggesting that the formation of these structures precedes AC and that they disassemble afterwards.

Although lens placodal AC is dependent on myosin activity, pharmacologically increasing myosin activity had no effect on either junctional displacement or AC. Interestingly, myosin activation resulted in an increase of lens placodal cells with actomyosin filaments and caused junctional myosin to pull away from apical junctions to varying degrees. These data are consistent with the idea that myosin activation is not sufficient for AC and requires a connection from the actomyosin filaments to apical junctions, which is a characteristic of invertebrate AC (Sawyer et al., 2009; Roh-Johnson et al., 2012). A junctional molecule is likely to be necessary for the AC machinery to associate itself with the ZA and this analysis implicates p120-catenin as fulfilling this role.

p120-catenin and Shroom3 are required for normal lens morphogenesis

Depletion of p120-catenin from the lens pit during invagination causes defects reminiscent of *Shroom3* mutant embryos, in which the lens pit loses curvature, has reduced AC and fails to form hinge points. A role for p120-catenin during early mouse eye morphogenesis is

Development (2014) 141, 3177-3187 doi:10.1242/dev.107433

consistent with other investigations showing that loss of p120-catenin causes eye defects in both *Drosophila* and *Xenopus* (Ciesiolka et al., 2004; Larson et al., 2008). In addition, ocular mesenchymal deletion of p120-catenin leads to anterior segment abnormalities in mice (Tian et al., 2012). Although these defects are attributed to altered morphogenesis, it remains unclear exactly how the tissues are affected. One noted possibility is the consistent loss of ZA proteins, such as cadherins and β-catenin, a finding common to most models of p120-catenin loss of function. No reduction in β-catenin localization in p120-catenin-deficient lens pits was observed, suggesting that these defects are not due to a loss of adhesive function. The quantitative assessment of cell shape and functional interaction with Shroom3 strongly suggest that p120-catenin, in conjunction with Shroom3, regulates AC. It is possible that the phenotypes observed in other models of p120-catenin depletion are in part due to a failure to regulate myosin contraction and/or AC. This is supported by the ability of RhoA and Rock to rescue the phenotype induced by p120-catenin depletion; both RhoA and Rock are necessary for Shroom3-dependent AC (Ciesiolka et al., 2004; Hildebrand, 2005; Plageman et al., 2011b).

The loss of hinge points in *Shroom3*$^{Gt/Gt}$ and *Shroom3*$^{+/Gt}$; *p120*$^{+/flox}$ mutants seems to lead to incomplete separation of the lens vesicle from the cornea, resulting in a Peters anomaly-like phenotype, commonly referred to as a persistent lens stalk. Intriguingly, although the curvature phenotype in the p120-catenin-deficient lens pits is very similar to both *Shroom3*$^{Gt/Gt}$ and *Shroom*$^{3+/Gt}$; *p120-catenin*$^{+/flox}$ mutants, we never observed incomplete separation. Therefore, an inhibition of AC and loss of lateral lens pit curvature is probably not the sole prerequisite for lens vesicle separation. This might be due to unidentified function(s) mediated by Shroom3 that are distinct from those involving p120-catenin. Several mouse mutants that display a similar lens stalk phenotype have disruptions in additional morphogenetic processes, such as proliferation, adhesion, differentiation and apoptosis, leaving open the possibility that Shroom3 might also function in these processes (Dimanlig et al., 2001; Ozeki et al., 2001; Medina-Martinez et al., 2005; Yoshimoto et al., 2005; Chen et al., 2008; Pontoriero et al., 2008, 2009; Kuracha et al., 2011; Cavalheiro et al., 2014).

Cooperative function of p120-catenin and Shroom3

The data presented here make a strong case for a cooperative function between Shroom3 and p120-catenin. In the absence of p120-catenin or in conditions in which p120-catenin cannot associate with cadherins, Shroom3 is unable to induce AC, presumably owing to a failure in Shroom3 ZA recruitment. The lack of junctional displacement in *Shroom3*$^{+/Gt}$; *p120*$^{+/flox}$ embryos and the reduction of apical Shroom3 localization in both p120-catenin mutants and in mutant N-cadherin-expressing A431D cells are consistent with this idea. A full complement of both proteins is necessary for AC and it might not occur in the doubly heterozygous embryos because the contractile activity induced by the remaining Shroom3 does not exert sufficient force on the partially p120-catenin-deficient ZA. A reduction of apical Shroom3 and myosin localization was also observed selectively in the hinge point-forming lateral margins, which is the region where curvature and AC are disrupted. It is possible that hinge point formation is preferentially affected due to the reduction of these proteins in this region; however, it is unclear why localization itself is regionally affected. Apical Shroom3 and p120-catenin localization appear uniform in the central and hinge point regions, eliminating the possibility that differential localization explains the regional phenotype. We have previously shown that Shroom3 plays a role in recruiting myosin apically in the lens, which might explain why myosin is affected (Plageman et al., 2010). The regional reduction in Shroom3 localization could be due to an unidentified protein that plays a compensatory role for p120-catenin in recruiting Shroom3 and resides exclusively in central lens pit cells. Alternatively, hinge point formation might simply be more sensitive to the AC machinery than the remainder of the lens pit. Although a significant contributor, AC is not the only driving force underlying lens pit invagination. There is evidence that mitosis, physical tethering of the lens pit to the coordinately bending optic vesicle by filopodia, and the extracellular matrix all contribute to this process (Hendrix and Zwaan, 1974; Chauhan et al., 2009; Huang et al., 2011). These forces might be more important in the central region, while significant contractile forces are necessary in the hinge points.

The ability of E-cadherin or β-catenin to recruit Shroom3 to the ZA was not tested; however, the high penetrance in *Shroom3*$^{+/Gt}$; *p120*$^{+/flox}$ embryos in contrast to the other doubly heterozygous combinations tested suggests that this recruitment occurs preferentially through p120-catenin rather than β-catenin and through N-cadherin rather than E-cadherin. The exclusivity of Shroom3 interaction with N-cadherin over E-cadherin might be related to the distinct role that each plays during epithelial morphogenesis (Kan et al., 2007; Nandadasa et al., 2009; Pontoriero et al., 2009). In the case of lens pit invagination, N-cadherin and p120-catenin could be the junctional components that mediate the linkage between the cortex-spanning actomyosin filaments and the ZA, whereas other cadherins and catenins play a more adhesive role.

Interestingly, doubly heterozygous *Shroom3*$^{+/Gt}$; *p120*$^{+/flox}$ embryos have an exacerbated cell shape phenotype, in which lens pit cells are significantly shorter and wider than either the *Shroom3* or p120-catenin homozygous mutants alone. This implies that for AC, half the normal levels of Shroom3 and p120-catenin protein is more detrimental to cells than the total loss of either protein. This might be explained by the role of additional proteins that regulate AC independently of Shroom3 and are at least partially dependent on p120-catenin. The reduction of both Shroom3 and p120-catenin protein levels might set up a scenario in which the local concentration of AC-triggering proteins is lowered at the ZA due to a decrease in their recruitment. It would be interesting to test whether the Lulu proteins, which can drive AC in the presence of dominant-negative Shroom3 (Nakajima and Tanoue, 2010; Chu et al., 2013), are similarly required for the cell shape changes necessary during lens pit invagination and are recruited to the ZA by p120-catenin.

Collectively, the data presented here implicate a role for ZA proteins, and especially p120-catenin, during vertebrate AC. Given the dependence of Shroom3 function on p120-catenin, and the similarity to the cortical organization of invertebrate apically constricting cells, it is surmised that vertebrate AC is driven at least partially by an apically positioned network of contractile actomyosin filaments that are anchored to the apical junctions and activated by Shroom3. To further define the mechanisms regulating AC will require the identification of additional components of the complex of proteins found at these anchorage points, how they are assembled and what triggers their assembly.

MATERIALS AND METHODS

Mouse line maintenance, embryonic dissection and embryo culture

The generation and maintenance of all lines utilized have been described previously: *p120-catenin*$^{flox/flox}$ (Davis and Reynolds, 2006), *E-cadherin*$^{flox/flox}$ (Boussadia et al., 2002), *β-catenin*$^{flox/flox}$ (Brault et al., 2001), *N-cadherin*$^{flox/flox}$ (Radice et al., 1997), *Shroom3*$^{Gt/Gt}$ (Hildebrand and Soriano, 1999) and *AP2α-cre* (Macatee et al., 2003). Embryos were removed from the uterus following hysterectomy, fixed in 4% paraformaldehyde and stored in PBS. Short-term mouse embryo culture was performed in 35 mm dishes containing

Development (2014) 141, 3177-3187 doi:10.1242/dev.107433

10% FBS/DMEM in the presence or absence of 100 µM (−)Blebbistatin (Sigma) or 5 nM Calyculin A (Santa Cruz) at 37°C for 90 min.

Immunolabeling

Histology and immunolabeling of cryosections, whole embryos and cultured cells were performed as previously described (Smith et al., 2005; Plageman et al., 2011b) utilizing the following primary and secondary antibodies and dilutions: rabbit anti-β-catenin (1:500; Santa Cruz, sc-7199), mouse anti-β-catenin (1:500; BD Biosciences, 610153), mouse anti-ZO1 (1:500; BD Biosciences, 610966), mouse anti-Flag (1:500; Sigma, F1804), mouse anti-Shroom3 (1:500), mouse anti-myosin IIb (1:5000; Covance, PRB445P), mouse anti-p120-catenin (1:200; BD Biosciences, 610133) and Alexa Fluor secondary antibodies (1:1000; Invitrogen, A21206, A11008, A21207, A11012, A11017, A21202, A21203, A11032). Phalloidin 488 (1:1000; Invitrogen, A12379) and Hoechst 33342 (1:1000; Sigma, B-2261) were used. Before Shroom3 immunolabeling, cryosections or whole embryos were immersed in 100 mM Tris pH 9.0 and heated in a preheated rice steamer for 30 (sections) or 10 (embryos) min.

DNA vector cloning, transfection and cell culture maintenance

To generate the R1838C mutation in Shroom3 the QuikChange site-directed mutagenesis kit (Agilent) was used with the primers 5′-CCTGCTGCT-GTCCCTGTCTGGATGCCTGGCCCGCGTGGAGAACG and its reverse complement and the Shroom3-Flag plasmid. Transient and stable MDCK and A431D transfections were performed utilizing TransIT-293 (Mirus, MIR 2700) according to the manufacturer's instructions. Stable MDCK cells expressing the shp120 vector (Dohn et al., 2009) were selected using 40 µg/ml puromycin and stable A431D cells expressing either N-cadherin-GFP (Addgene, 18870) or 1099-N-cadherin-AAA-YFP (Addgene, 32237) were selected with 400 µg/ml G418 (Sigma, G8168). Cells were fixed 48 h after transient transfection of ∼30% confluent cells with 0.5 µg of the indicated plasmid.

Morphometric analysis

Lens pit cell shape was determined as previously described (Plageman et al., 2010, 2011b). For each genotype at least three images of centrally positioned cryosections of each eye were used from three to eight different embryos. Quantitative data for the *Shroom3*$^{Gt/Gt}$ cell shape have been published previously (Plageman et al., 2010).

Apical and basal areas based on β-catenin/ZO-1/N-cadherin/F-actin staining were quantified by tracing the outer junctional signal using ImageJ (1.46R). Each experiment was performed at least three times and the averages are based on pooled values from all cells measured.

To determine filament angles, the Angle tool of ImageJ was used to draw an angle from a central point in the lens placode to the central point of a single prominent filament per cell and along the filament in a clockwise direction. Averages were calculated from all cells within three placodes.

Junctional displacement measurements were performed on at least seven junctions per lens placode from at least three embryos per genotype or experimental group. A straight line was drawn between two tricellular junctions joined by a bicellular junction apically associated with a myosin IIb-labeled filament(s) at the inner side of the β-catenin signal. Junctions with filaments associated with opposite sides of the bicellular junction were excluded from the analysis. Length measurements utilizing ZEN software (Zeiss) were performed between and perpendicular to the drawn line and the outer edge of the bicellular junctional β-catenin signal where the myosin filament is associated.

The average (x,y) coordinates were determined by tracing the apical and basal surface in Adobe Photoshop (CS6) from images of central lens pit sections from six to eight embryos, anchoring the basal traces to the bottom mid-point and utilizing ImageJ to generate the coordinates for each tracing curvature at a given coordinate (x,y), which was calculated from the inverse of a circle passing through point (x,y) and the coordinates of its neighboring points using the formula:

$$\frac{1}{\sqrt{(x-x_c)^2+(y+y_c)^2}},$$

where x_c and y_c are coordinates of the center of the circle. Point (x_c,y_c) was derived from the equations:

$$x_c = \frac{m_1 m_2 (y_1 - y_3) + m_2 (x_1 + x_2) - m_1 (x_2 + x_3)}{2(m_2 - m_1)}$$

and

$$y_c = \frac{1}{m_1}\left(x - \frac{x_1 + x_2}{2}\right) + \frac{y_1 + y_2}{2},$$

where (x_1,y_1) and (x_3,y_3) are the neighboring points to (x_2,y_2). Curvature trendlines were generated using Microsoft Excel (sixth order polynomial). The average curvature values were determined by averaging all of the values generated from equivalent line segments of the left, right or central regions of lens pits.

Immunofluorescence intensity measurements

Using ImageJ, the average fluorescence intensity was measured along a 31-pixel interval perpendicular to the junctional direction of two adjacent cells with N-cadherin (A431D cells) or p120-catenin (lens sections) labeling. For p120-catenin, the raw values of eight junctions from three to eight embryos were divided by the minimum intensity value for each line segment and averaged. For A431D cells, five to ten cell pairs were measured at five unique intervals in each experimental group, and the lowest value (MIN) among all raw pixel intensity values (RAW) derived from the same image was determined. Data were normalized by calculating RAW/MIN and averaged. The average Shroom3, myosin IIb and F-actin signal was determined using ImageJ to outline the apical areas of the central (bottom two-thirds of apical surface) or hinge point (upper third) regions of immunolabeled cryosections, and normalizing the raw values to the average intensity of the whole lens pit.

Statistics

Based on the Shapiro–Wilk test, all quantitative data sets were determined to be non-normally distributed and significant differences between data points were therefore determined from the non-parametric Mann–Whitney *U*-test. All statistical analyses were performed using SPSS (IBM, version 19); not all statistically significant differences are noted.

Acknowledgements

We thank Paul Speeg for excellent technical assistance.

Competing interests

The authors declare no competing financial interests.

Author contributions

T.F.P., J.D.H., R.A.L. and A.B.R. developed the approach; T.F.P. and K.H. performed experiments; T.F.P. prepared the manuscript.

Funding

We acknowledge grant support from the National Institutes of Health [R01 EY016241] and from the Abrahamson Pediatric Eye Institute of the Children's Hospital Medical Center of Cincinnati to R.A.L.; and the National Institutes of Health [5R01 GM102524 to A.B.R., and R01 GM067525 to J.D.H.]. Deposited in PMC for release after 12 months.

Supplementary material

Supplementary material available online at
http://dev.biologists.org/lookup/suppl/doi:10.1242/dev.107433/-/DC1

References

Boussadia, O., Kutsch, S., Hierholzer, A., Delmas, V. and Kemler, R. (2002). E-cadherin is a survival factor for the lactating mouse mammary gland. *Mech. Dev.* **115**, 53-62.

Brault, V., Moore, R., Kutsch, S., Ishibashi, M., Rowitch, D. H., McMahon, A. P., Sommer, L., Boussadia, O. and Kemler, R. (2001). Inactivation of the beta-catenin gene by Wnt1-Cre-mediated deletion results in dramatic brain malformation and failure of craniofacial development. *Development* **128**, 1253-1264.

Cavalheiro, G. R., Matos-Rodrigues, G. E., Gomes, A. L., Rodrigues, P. M. G. and Martins, R. A. P. (2014). c-myc regulates cell proliferation during lens development. *PLoS ONE* **9**, e87182.

Chauhan, B. K., Disanza, A., Choi, S.-Y., Faber, S. C., Lou, M., Beggs, H. E., Scita, G., Zheng, Y. and Lang, R. A. (2009). Cdc42- and IRSp53-dependent contractile filopodia tether presumptive lens and retina to coordinate epithelial invagination. *Development* **136**, 3657-3667.

Chauhan, B. K., Lou, M., Zheng, Y. and Lang, R. A. (2011). Balanced Rac1 and RhoA activities regulate cell shape and drive invagination morphogenesis in epithelia. *Proc. Natl. Acad. Sci. USA* **108**, 18289-18294.
Chen, Y., Doughman, Y.-Q., Gu, S., Jarrell, A., Aota, S.-I., Cvekl, A., Watanabe, M., Dunwoodie, S. L., Johnson, R. S., van Heyningen, V. et al. (2008). Cited2 is required for the proper formation of the hyaloid vasculature and for lens morphogenesis. *Development* **135**, 2939-2948.
Chu, C.-W., Gerstenzang, E., Ossipova, O. and Sokol, S. Y. (2013). Lulu regulates Shroom-induced apical constriction during neural tube closure. *PLoS ONE* **8**, e81854.
Ciesiolka, M., Delvaeye, M., Van Imschoot, G., Verschuere, V., McCrea, P., van Roy, F. and Vleminckx, K. (2004). p120 catenin is required for morphogenetic movements involved in the formation of the eyes and the craniofacial skeleton in Xenopus. *J. Cell Sci.* **117**, 4325-4339.
David, D. J. V., Tishkina, A. and Harris, T. J. C. (2010). The PAR complex regulates pulsed actomyosin contractions during amnioserosa apical constriction in Drosophila. *Development* **137**, 1645-1655.
Davis, M. A. and Reynolds, A. B. (2006). Blocked acinar development, E-cadherin reduction, and intraepithelial neoplasia upon ablation of p120-catenin in the mouse salivary gland. *Dev. Cell* **10**, 21-31.
Dimanlig, P. V., Faber, S. C., Auerbach, W., Makarenkova, H. P. and Lang, R. A. (2001). The upstream ectoderm enhancer in Pax6 has an important role in lens induction. *Development* **128**, 4415-4424.
Dohn, M. R., Brown, M. V. and Reynolds, A. B. (2009). An essential role for p120-catenin in Src- and Rac1-mediated anchorage-independent cell growth. *J. Cell Biol.* **184**, 437-450.
Hendrix, R. W. and Zwaan, J. (1974). Cell shape regulation and cell cycle in embryonic lens cells. *Nature* **247**, 145-147.
Hildebrand, J. D. (2005). Shroom regulates epithelial cell shape via the apical positioning of an actomyosin network. *J. Cell Sci.* **118**, 5191-5203.
Hildebrand, J. D. and Soriano, P. (1999). Shroom, a PDZ domain-containing actin-binding protein, is required for neural tube morphogenesis in mice. *Cell* **99**, 485-497.
Huang, J., Rajagopal, R., Liu, Y., Dattilo, L. K., Shaham, O., Ashery-Padan, R. and Beebe, D. C. (2011). The mechanism of lens placode formation: a case of matrix-mediated morphogenesis. *Dev. Biol.* **355**, 32-42.
Huelsken, J., Vogel, R., Brinkmann, V., Erdmann, B., Birchmeier, C. and Birchmeier, W. (2000). Requirement for beta-catenin in anterior-posterior axis formation in mice. *J. Cell Biol.* **148**, 567-578.
Iioka, H., Ueno, N. and Kinoshita, N. (2004). Essential role of MARCKS in cortical actin dynamics during gastrulation movements. *J. Cell Biol.* **164**, 169-174.
Kan, N. G., Stemmler, M. P., Junghans, D., Kanzler, B., de Vries, W. N., Dominis, M. and Kemler, R. (2007). Gene replacement reveals a specific role for E-cadherin in the formation of a functional trophectoderm. *Development* **134**, 31-41.
Kim, H. Y., Varner, V. D. and Nelson, C. M. (2013). Apical constriction initiates new bud formation during monopodial branching of the embryonic chicken lung. *Development* **140**, 3146-3155.
Koleske, A. J., Gifford, A. M., Scott, M. L., Nee, M., Bronson, R. T., Miczek, K. A. and Baltimore, D. (1998). Essential roles for the Abl and Arg tyrosine kinases in neurulation. *Neuron* **21**, 1259-1272.
Kuracha, M. R., Burgess, D., Siefker, E., Cooper, J. T., Licht, J. D., Robinson, M. L. and Govindarajan, V. (2011). Spry1 and Spry2 are necessary for lens vesicle separation and corneal differentiation. *Invest. Ophthalmol. Vis. Sci.* **52**, 6887-6897.
Larson, D. E., Liberman, Z. and Cagan, R. L. (2008). Cellular behavior in the developing Drosophila pupal retina. *Mech. Dev.* **125**, 223-232.
Lee, C., Scherr, H. M. and Wallingford, J. B. (2007). Shroom family proteins regulate gamma-tubulin distribution and microtubule architecture during epithelial cell shape change. *Development* **134**, 1431-1441.
Macatee, T. L., Hammond, B. P., Arenkiel, B. R., Francis, L., Frank, D. U. and Moon, A. M. (2003). Ablation of specific expression domains reveals discrete functions of ectoderm- and endoderm-derived FGF8 during cardiovascular and pharyngeal development. *Development* **130**, 6361-6374.
Marean, A., Graf, A., Zhang, Y. and Niswander, L. (2011). Folic acid supplementation can adversely affect murine neural tube closure and embryonic survival. *Hum. Mol. Genet.* **20**, 3678-3683.
Martin, A. C., Kaschube, M. and Wieschaus, E. F. (2009). Pulsed contractions of an actin-myosin network drive apical constriction. *Nature* **457**, 495-499.
Martin, A. C., Gelbart, M., Fernandez-Gonzalez, R., Kaschube, M. and Wieschaus, E. F. (2010). Integration of contractile forces during tissue invagination. *J. Cell Biol.* **188**, 735-749.
Mason, F. M., Tworoger, M. and Martin, A. C. (2013). Apical domain polarization localizes actin-myosin activity to drive ratchet-like apical constriction. *Nat. Cell Biol.* **15**, 926-936.
Massarwa, R. and Niswander, L. (2013). In toto live imaging of mouse morphogenesis and new insights into neural tube closure. *Development* **140**, 226-236.
McCrea, P. D. and Park, J.-I. (2007). Developmental functions of the P120-catenin sub-family. *Biochim. Biophys. Acta* **1773**, 17-33.
Medina-Martinez, O., Brownell, I., Amaya-Manzanares, F., Hu, Q., Behringer, R. R. and Jamrich, M. (2005). Severe defects in proliferation and differentiation of lens cells in Foxe3 null mice. *Mol. Cell. Biol.* **25**, 8854-8863.
Mohan, S., Rizaldy, R., Das, D., Bauer, R. J., Heroux, A., Trakselis, M. A., Hildebrand, J. D. and VanDemark, A. P. (2012). Structure of Shroom domain 2 reveals a three-segmented coiled-coil required for dimerization, Rock binding, and apical constriction. *Mol. Biol. Cell* **23**, 2131-2142.
Morita, H., Nandadasa, S., Yamamoto, T. S., Terasaka-Iioka, C., Wylie, C. and Ueno, N. (2010). Nectin-2 and N-cadherin interact through extracellular domains and induce apical accumulation of F-actin in apical constriction of Xenopus neural tube morphogenesis. *Development* **137**, 1315-1325.
Nakajima, H. and Tanoue, T. (2010). Epithelial cell shape is regulated by Lulu proteins via myosin-II. *J. Cell Sci.* **123**, 555-566.
Nandadasa, S., Tao, Q., Menon, N. R., Heasman, J. and Wylie, C. (2009). N- and E-cadherins in Xenopus are specifically required in the neural and non-neural ectoderm, respectively, for F-actin assembly and morphogenetic movements. *Development* **136**, 1327-1338.
Ozeki, H., Ogura, Y., Hirabayashi, Y. and Shimada, S. (2001). Suppression of lens stalk cell apoptosis by hyaluronic acid leads to faulty separation of the lens vesicle. *Exp. Eye Res.* **72**, 63-70.
Pieters, T., van Hengel, J. and van Roy, F. (2012). Functions of p120ctn in development and disease. *Front. Biosci.* **17**, 760-783.
Plageman, T. F., Jr, Chung, M.-I., Lou, M., Smith, A. N., Hildebrand, J. D., Wallingford, J. B. and Lang, R. A. (2010). Pax6-dependent Shroom3 expression regulates apical constriction during lens placode invagination. *Development* **137**, 405-415.
Plageman, T. F., Jr, Zacharias, A. L., Gage, P. J. and Lang, R. A. (2011a). Shroom3 and a Pitx2-N-cadherin pathway function cooperatively to generate asymmetric cell shape changes during gut morphogenesis. *Dev. Biol.* **357**, 227-234.
Plageman, T. F., Jr, Chauhan, B. K., Yang, C., Jaudon, F., Shang, X., Zheng, Y., Lou, M., Debant, A., Hildebrand, J. D. and Lang, R. A. (2011b). A Trio-RhoA-Shroom3 pathway is required for apical constriction and epithelial invagination. *Development* **138**, 5177-5188.
Pontoriero, G. F., Deschamps, P., Ashery-Padan, R., Wong, R., Yang, Y., Zavadil, J., Cvekl, A., Sullivan, S., Williams, T. and West-Mays, J. A. (2008). Cell autonomous roles for AP-2alpha in lens vesicle separation and maintenance of the lens epithelial cell phenotype. *Dev. Dyn.* **237**, 602-617.
Pontoriero, G. F., Smith, A. N., Miller, L.-A. D., Radice, G. L., West-Mays, J. A. and Lang, R. A. (2009). Co-operative roles for E-cadherin and N-cadherin during lens vesicle separation and lens epithelial cell survival. *Dev. Biol.* **326**, 403-417.
Radice, G. L., Rayburn, H., Matsunami, H., Knudsen, K. A., Takeichi, M. and Hynes, R. O. (1997). Developmental defects in mouse embryos lacking N-cadherin. *Dev. Biol.* **181**, 64-78.
Roffers-Agarwal, J., Xanthos, J. B., Kragtorp, K. A. and Miller, J. R. (2008). Enabled (Xena) regulates neural plate morphogenesis, apical constriction, and cellular adhesion required for neural tube closure in Xenopus. *Dev. Biol.* **314**, 393-403.
Roh-Johnson, M., Shemer, G., Higgins, C. D., McClellan, J. H., Werts, A. D., Tulu, U. S., Gao, L., Betzig, E., Kiehart, D. P. and Goldstein, B. (2012). Triggering a cell shape change by exploiting preexisting actomyosin contractions. *Science* **335**, 1232-1235.
Sawyer, J. K., Harris, N. J., Slep, K. C., Gaul, U. and Peifer, M. (2009). The Drosophila afadin homologue Canoe regulates linkage of the actin cytoskeleton to adherens junctions during apical constriction. *J. Cell Biol.* **186**, 57-73.
Sawyer, J. M., Harrell, J. R., Shemer, G., Sullivan-Brown, J., Roh-Johnson, M. and Goldstein, B. (2010). Apical constriction: a cell shape change that can drive morphogenesis. *Dev. Biol.* **341**, 5-19.
Simoes Sde, M., Mainieri, A. and Zallen, J. A. (2014). Rho GTPase and Shroom direct planar polarized actomyosin contractility during convergent extension. *J. Cell Biol.* **204**, 575-589.
Smith, A. N., Miller, L.-A. D., Song, N., Taketo, M. M. and Lang, R. A. (2005). The duality of beta-catenin function: a requirement in lens morphogenesis and signaling suppression of lens fate in periocular ectoderm. *Dev. Biol.* **285**, 477-489.
Smith, A. L., Dohn, M. R., Brown, M. V. and Reynolds, A. B. (2012). Association of Rho-associated protein kinase 1 with E-cadherin complexes is mediated by p120-catenin. *Mol. Biol. Cell* **23**, 99-110.
Solon, J., Kaya-Copur, A., Colombelli, J. and Brunner, D. (2009). Pulsed forces timed by a ratchet-like mechanism drive directed tissue movement during dorsal closure. *Cell* **137**, 1331-1342.
Somlyo, A. P. and Somlyo, A. V. (2000). Signal transduction by G-proteins, rho-kinase and protein phosphatase to smooth muscle and non-muscle myosin II. *J. Physiol.* **522**, 177-185.
Suzuki, M., Morita, H. and Ueno, N. (2012). Molecular mechanisms of cell shape changes that contribute to vertebrate neural tube closure. *Dev. Growth Differ.* **54**, 266-276.
Tian, H., Sanders, E., Reynolds, A., van Roy, F. and van Hengel, J. (2012). Ocular anterior segment dysgenesis upon ablation of p120 catenin in neural crest cells. *Invest. Ophthalmol. Vis. Sci.* **53**, 5139-5153.
Xu, W., Baribault, H. and Adamson, E. D. (1998). Vinculin knockout results in heart and brain defects during embryonic development. *Development* **125**, 327-337.
Yoshimoto, A., Saigou, Y., Higashi, Y. and Kondoh, H. (2005). Regulation of ocular lens development by Smad-interacting protein 1 involving Foxe3 activation. *Development* **132**, 4437-4448.

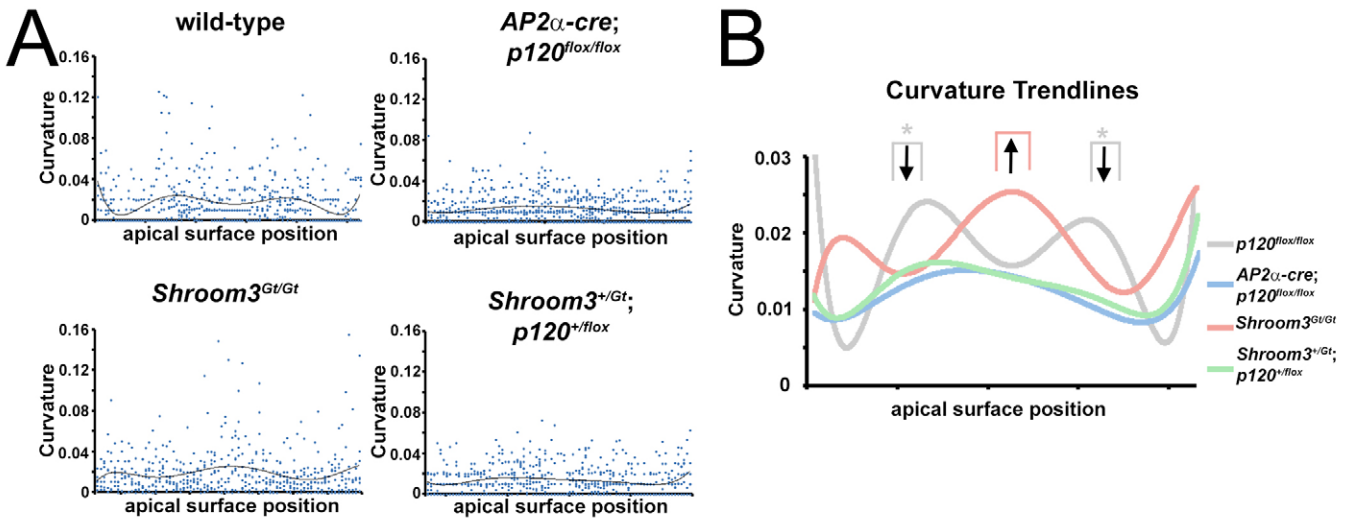

Figure S1. Curvature data for (x,y) coordinates. (A) Representation of all apical curvature values generated from the (x,y) coordinates of 6-8 central lens pit sections from the indicated genotype. The black line in each graph represents a 6th order polynomial trendline. (B) Comparison of the trendlines generated in (A) were placed on the same graph with an expanded y axis. The brackets indicate curvature values used for the quantification and statistical analysis for Figure 4C, and the asterisks represent a significant difference compared with the control genotype.

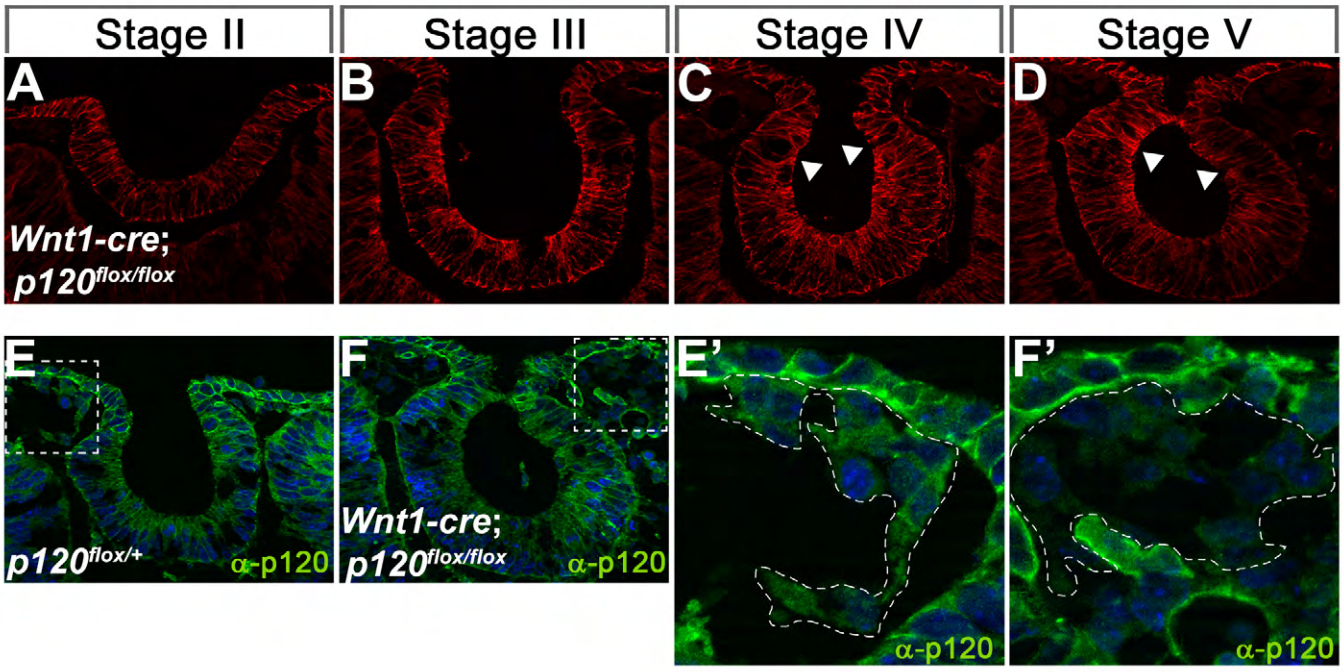

Figure S2. Mesenchymal deletion of p120-catenin does not affect lens pit morphogenesis. (A-D) Cryosectioned E10.5 mouse embryo eyes (stages II-V) deficient for p120-catenin in the mesenchyme during lens pit invagination were immunolabeled with a β-catenin (red). Note the formation of the lens pit hinge-points in C and D (white arrowheads). (E-F) Control or p120-catenin mesenchymal deficient eyes were immunolabeled with p120 catenin (green) and Hoeschst (blue). The white dashed square is magnified in the left panels (E',F'). Ocular mesenchyme is outlined to highlight the presence (E') or absence (F') of p120-catenin labeling.

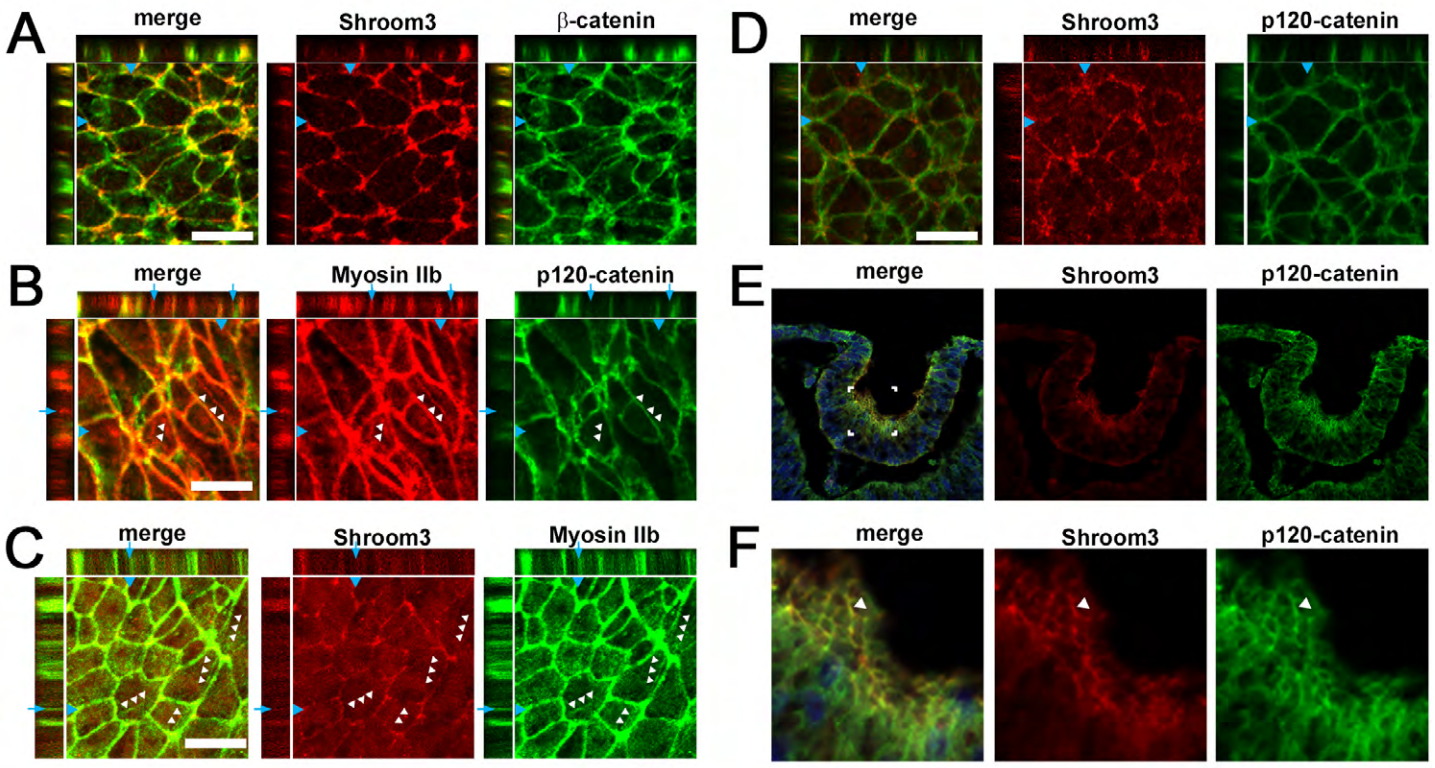

Figure S3. Shroom3 and p120-catenin localization in the lens placode and lens pit. (A-D) Representative *en face* view of immunolabeled lens placodes utilizing the indicated antibodies. White arrowheads and colored arrows indicate the location of myosin filaments. (E-F) Lens pit colabeled with Shroom3 and p120-catenin at lower (E) and higher magnification (F). Scalebars: 5 mm.